



OPEN

Integrated genomics point to immune vulnerabilities in pleural mesothelioma

Anca Nastase^{1,12}, Amit Mandal^{1,12}, Shir Kiong Lu¹, Hima Anbunathan¹, Deborah Morris-Rosendahl^{1,2}, Yu Zhi Zhang^{1,3}, Xiao-Ming Sun⁴, Spyridon Gennatas¹, Robert C. Rintoul^{5,6}, Matthew Edwards², Alex Bowman³, Tatyana Chernova⁴, Tim Benepal⁷, Eric Lim⁸, Anthony Newman Taylor¹, Andrew G. Nicholson^{1,3}, Sanjay Popat^{9,10}, Anne E. Willis⁴, Marion MacFarlane⁴, Mark Lathrop¹¹, Anne M. Bowcock¹, Miriam F. Moffatt^{1,13}✉ & William O. C. M. Cookson^{1,13}✉

Pleural mesothelioma is an aggressive malignancy with limited effective therapies. In order to identify therapeutic targets, we integrated SNP genotyping, sequencing and transcriptomics from tumours and low-passage patient-derived cells. Previously unrecognised deletions of *SUFU* locus (10q24.32), observed in 21% of 118 tumours, resulted in disordered expression of transcripts from Hedgehog pathways and the T-cell synapse including *VISTA*. Co-deletion of Interferon Type I genes and *CDKN2A* was present in half of tumours and was a predictor of poor survival. We also found previously unrecognised deletions in *RB1* in 26% of cases and show sub-micromolar responses to downstream *PLK1*, *CHEK1* and Aurora Kinase inhibitors in primary mesothelioma cells. Defects in Hippo pathways that included *RASSF7* amplification and *NF2* or *LATS1/2* mutations were present in 50% of tumours and were accompanied by micromolar responses to the YAP1 inhibitor Verteporfin. Our results suggest new therapeutic avenues in mesothelioma and indicate targets and biomarkers for immunotherapy.

Pleural mesothelioma is an aggressive malignancy associated with asbestos exposure. Global mesothelioma deaths are estimated to be 38,400 each year¹. Mesothelioma is usually refractory to known treatments. Although 20% of tumours may transiently regress after checkpoint immunotherapy^{2,3}, PD-L1 is expressed at a low level in the majority of mesothelioma cases³ and predictors of response are unknown. The molecular landscape is not complex but to date known recurrent lesions have not yet defined effective therapeutic targets^{4,5}.

Intense fibrosis typically accompanies mesothelioma and may cause intractable pain and dyspnoea. For example, in the UK Mesobank tumour repository⁶ 65% of mesothelioma have < 25% of tumour cells visible on surgical biopsy and only 8% of mesothelioma comprise > 75% malignant cells. This suggests the tumour-matrix interaction to be a feature of the disease.

Inflammation and fibrosis in the pleura are normally adaptive mechanisms that seal off foci of injury or infection. Incomplete macrophage phagocytosis of inhaled high-aspect ratio asbestos fibres induces sustained inflammation and cytokine release^{7,8}, increased mesothelial proliferation, oxidative DNA damage⁹ and double strand DNA breakages¹⁰ that can cause malignant transformation.

Previous genomic analyses of mesothelioma have shown a mutational landscape dominated by loss of function mutations in *BAP1* and *NF2*^{4,5}. Larger structural variations in mesothelioma are common¹¹, and recurrent deletions are recognised for *CDKN2A* (located at chromosome 9p21.3), *NF2* (22q12) and *BAP1* (3p21.3).

¹National Heart and Lung Institute, Imperial College London, Dovehouse Street, London SW36LY, UK. ²Clinical Genetics and Genomics, Royal Brompton and Harefield NHS Foundation Trust, London, UK. ³Department of Histopathology, Royal Brompton and Harefield NHS Foundation Trust, London, UK. ⁴Medical Research Council Toxicology Unit, University of Cambridge, Cambridge, UK. ⁵Department of Thoracic Oncology, Papworth Hospital, Cambridge, UK. ⁶Department of Oncology, University of Cambridge, Cambridge, UK. ⁷Department of Oncology, St George's Healthcare NHS Foundation Trust, London, UK. ⁸Department of Thoracic Surgery, Royal Brompton and Harefield NHS Foundation Trust, London, UK. ⁹Department of Medicine, Royal Marsden Hospital, London, UK. ¹⁰The Institute of Cancer Research, London, UK. ¹¹Department of Human Genetics, McGill Genome Centre, Montreal, QC, Canada. ¹²These authors contributed equally: Anca Nastase and Amit Mandal. ¹³These authors jointly supervised this work: Miriam Moffatt and William Cookson. ✉email: m.moffatt@imperial.ac.uk; w.cookson@imperial.ac.uk

Given the proclivity for asbestos to induce DNA damage, we extended genomic findings in 121 mesothelioma tumours by fine mapping of copy-number alterations (CNAs) with high-density SNP arrays. We explored the mutational spectrum with whole exome sequencing (WES) in 50 subjects (21 of which had paired blood samples for germline DNA), before extending mutation detection to all tumours with a 57-gene targeted capture next-generation sequencing (TC-NGS) panel (Supplementary File 1_Fig. 1a, b and Supplementary File 1_Table 1). In addition, we whole-genome sequenced (WGS) 19 low-passage primary mesothelioma derived cell cultures (PMCC)¹².

Results

Demographic and clinical characteristics. One hundred and five of the 121 patients (87%) were male (Supplementary File 1_Table 2). Ninety tumours exhibited the epithelioid subtype of mesothelioma, 25 were biphasic and 6 were sarcomatoid (Supplementary File 1_Fig. 1c). Patients with sarcomatoid disease were older than the other two groups ($P=0.05$). Asbestos exposure had been documented clinically in 69% of cases. The median overall survival (OS) for all subjects was 9.9 months with sarcomatoid patients showing a worse outcome than others, ($P=0.065$) (survival time from diagnosis to death or last follow-up was available for 110 patients; Supplementary File 1_Table 2 and Supplementary File 1_Fig. 1d; Supplementary File 2_Table 1), as described¹³.

Given the wide variability between the proportions of mesothelioma malignant cells and matrix fibrosis, we estimated the tumour content of all samples with ASCAT analysis of the > 950 K SNPs in the Illumina Infinium OmniExpressExome-8 v1.3 and v1.4 panels. We found the median tumour content was 0.44 (range 0.2–1.0; 1st quartile 0.32; 3rd quartile 0.9; median absolute deviation 0.22).

Copy number alterations (CNAs) analysis shows recurrent *CDKN2A*, *RB1* and *SUFU* deletion and *RASSF7* amplification. We analysed the SNPs for CNAs using the GISTIC program¹⁴. The program estimates genomic boundaries for recurrent CNA events and assigns statistical significance after false discovery rate (FDR) corrections.

Deletion of *CDKN2A* was the most frequent event observed in our samples, detected in 71/118 tumours (60%), with 58 deletions (82%) predicted to be homozygous (Figs. 1a, 2). As previously reported¹⁵, *CDKN2A* deletion was associated with worse OS compared with *CDKN2A* wild type patients (8.8 vs 13.0 months, Kaplan–Meier $P=0.02$) (Fig. 1c), and with increased copy number burden (Supplementary File 2_Table 5A).

Deletion of the *CDKN2A* region is extensive in many malignancies and a full locus map (Fig. 1b) revealed large deletions to also be present in mesothelioma. The map revealed a frequent deletion of the closely neighbouring Type I Interferon (IFN) genes, as we have first reported¹⁶ and has later been confirmed¹⁷ (Fig. 1b and Supplementary File 2_Table 6): 38/118 patients (32%) had predicted homozygous IFN Type I deletion and 24/118 (20%) had heterozygous deletion. The median survival of patients with co-deletion of *CDKN2A* and IFN Type I genes was not statistically different to *CDKN2A* deletions alone (8.3 months compared to 10.7, $P=0.6$; Supplementary File 2_Table 6).

We observed frequent deletions at multiple other loci (Fig. 1d–f, Supplementary File 1_Table 3 and Supplementary File 2_Table 5B for the extensive list of copy-number coordinates for each sample). The most common novel deletion was the *RB1* locus on 13q14.2 in 31/118 patients (26%). The *RB1* tumour suppressor is activated downstream of CDK4 and CDK6¹⁸ and its deletion predicts a mechanism for resistance to CDK4/6 inhibitors.

Deletion of a locus on 10q24.32 containing *SUFU* (Suppressor of Fused), *ARL3* (ADP Ribosylation Factor Like GTPase 3) and *TRIM8* (Tripartite Motif Containing 8) was observed in 25/118 tumours (21%). *SUFU* inhibits activation of GLI transcription factors in the Hedgehog pathway, which is known to be disordered during mesothelioma carcinogenesis^{19,20}. *TRIM8* acts as a tumour suppressor inducing cell cycle arrest in a TP53 dependant manner, and as an oncogene activating NF- κ B and TNF- α ²¹. It is involved both in immunity and cancer²².

Previously unrecognised regions of amplification (Figs. 1a, 2, Supplementary File 1_Table 3 and Supplementary File 2_Table 5B for the extensive list of copy-number coordinates for each sample) included a locus on 11p15.5, amplified in 39/118 tumours (33%) that contained *RASSF7* and *miR-210* (Fig. 1g). When up-regulated *RASSF7* controls cell growth and apoptosis in different tumours²³, and functions as an oncogene in NSCLC, interacting with *MST1* to dysregulate Hippo signalling²⁴.

Other substantial amplifications included 19q13.43 in 24/118 tumours (20%), containing *NLRP5*, *ZNF444* and *ZNF787*; 5q35.2 in 27/118 tumours (23%), containing *GPRIN1* immediately adjacent to *CDHR2* which may moderate contact inhibition of epithelial cell growth²⁵; and 5q35.3 in 26/118 tumours (22%) containing *LTC4S* and *SQSTM1*. The latter encodes p62, a mediator of autophagy influencing tumorigenesis, malignant growth and resistance to therapy²⁶.

We sought replication of the novel CNAs in 98 tumours from the landmark study of Bueno et al.⁵ which carried out WES and concurrent RNA-sequencing. We confirmed amplification of *RASSF7* and deletion of *RB1* and *SUFU*, each of which correlated with its transcript abundance (Supplementary File 1_Fig. 4 and Supplementary File 2_Table 7).

Deletion of *SUFU* locus, component of Hedgehog signalling pathway, is associated with downregulation of immune related genes. Deletion of the *SUFU* locus in 25/118 tumours (21%) was associated with marked upregulation of the *Patched 2* tumour suppressor (*PTCH2*) (Table 1). *Ptch2* overexpression has been observed in *Sufu* knockout mice and is indicative of aberrant Hedgehog signalling²⁰. Hedgehog pathways are activated in mesothelioma patients, in the absence of obvious mutations¹⁹. Also, upregulated were *NHS*, *HOXA7* and *TRPS1*, each of which regulate tissue differentiation (Table 1).

We found a SMO (Smoothed) inhibitor (Vismodegib, GDC-0499) to be inhibitory in only one PMCC (Table 2). Vismodegib has previously been shown to be effective in modulating mesothelioma tumour and

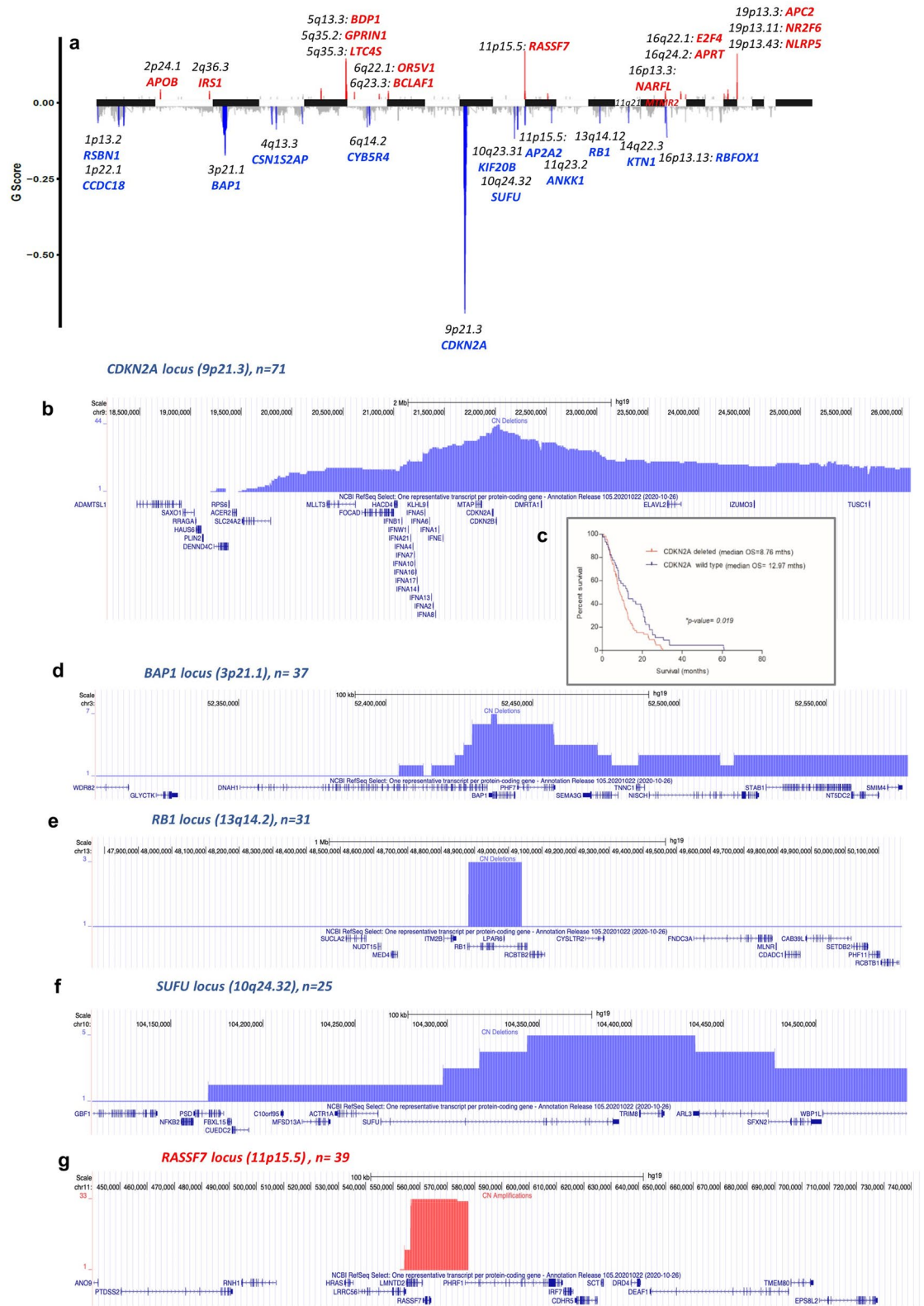


Figure 1. Mapping of copy number alterations in subjects with pleural mesothelioma. (a) Statistically significant regions of amplification and deletion from GISTIC analysis of 118 subjects. Peak regions which pass both the G-Score (Gistic score in ver.2.0 is defined as the negative logarithm of the probability of observing a candidate copy-number segment with given amplitude and frequency, provided the background copy-number alteration rate) and q-bound (<0.05) threshold cut-offs are shown for deletions (blue) and amplifications (red) (see also Supplementary File 1_Table 3 and Supplementary File 2_Table 5B for the extensive list of copy-number segment coordinates for each sample); (b) Detailed map of the *CDKN2A* locus using the UCSC Genome Browser (hg19), showing histogram representation of overlap among deletion segments from the 118 subjects. *IFN* Type I genes are commonly within the deleted segments; (c) Kaplan–Meier survival analysis of patients with and without *CDKN2A* locus deletions; (d–f) Similar Genome Browser based maps of the *BAP1*, *RB1* and *SUFU* deleted segments; (g) Map for amplification segments from the *RASSF7* locus.

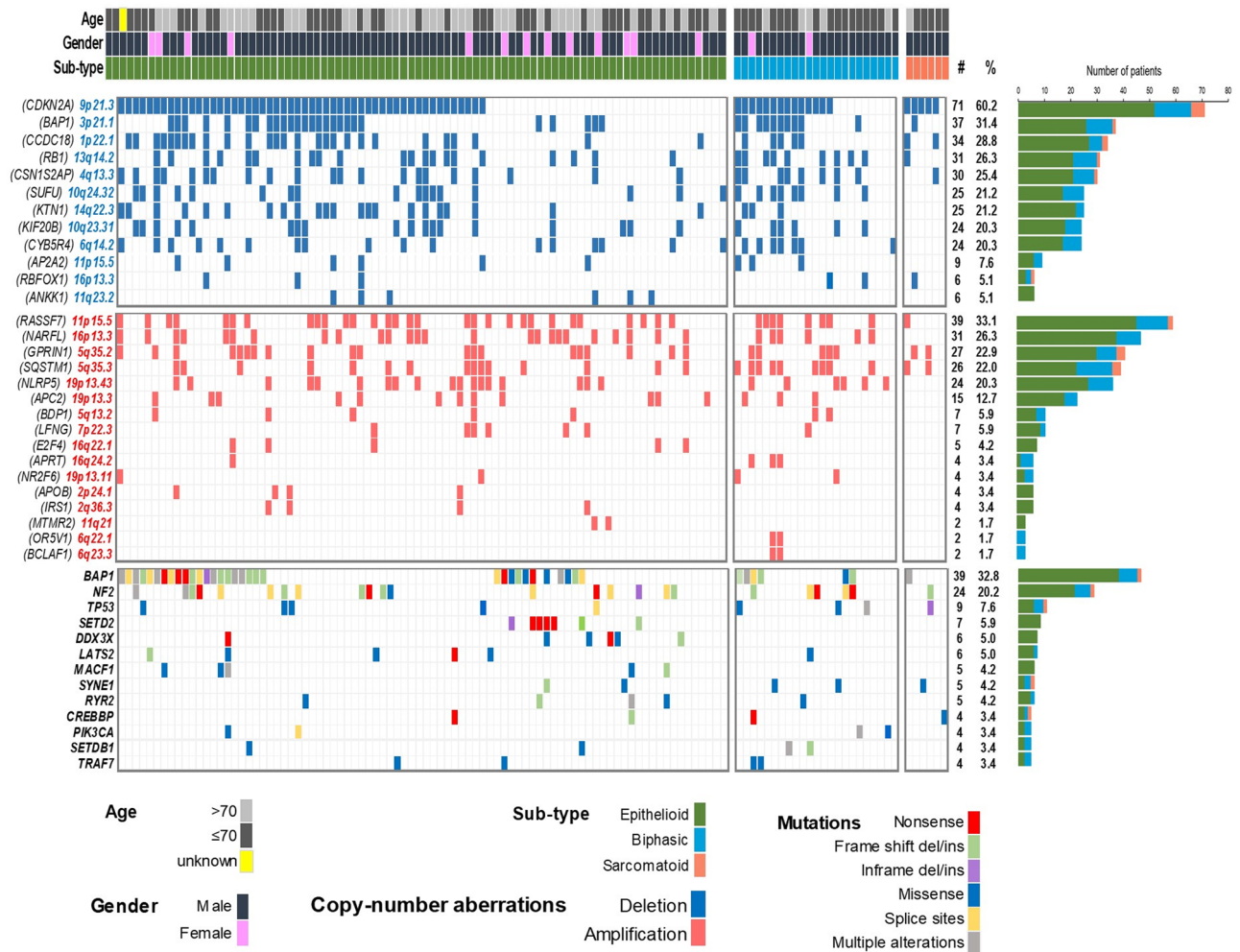


Figure 2. Common genetic alterations in Pleural Mesothelioma. The most common deletions (top panel), amplifications (middle panel) and mutations (bottom panel) are shown in 118 subjects. CNA analyses are derived from SNP arrays and mutated genes from the targeted capture sequencing panel.

stromal interactions in a rat model of mesothelioma²⁷, suggesting beneficial effects of Hedgehog inhibition would be worthy of investigation in mixed cellular cultures of human mesothelioma.

SUFU deletion unexpectedly correlated with downregulation of prominent T-cell genes (Table 1), including *ODF3B*; the killer-cell receptor *KLRD1* (*CD94*); and *HSH2D*, a target of T-cell activation. Downregulated monocyte/macrophage and dendritic cell markers included *IL4R*, *SCIMP*, *SIGLEC1* (*CD169*), *CLEC10A*, and *CR1* (Complement C3b/C4b receptor 1).

We confirmed these results in the large independent dataset from Bueno et al.⁵, confirming that abundances of Hedgehog pathway transcripts *SUFU*, *PTCH1* and *PTCH2* correlated with *KLRD1* and *CR1* (Supplementary File 1_Table 5).

Hippo pathway is deregulated in 50% of mesothelioma patients due to *RASSF7* amplification and *NF2*, *LATS1/2* mutations. Hippo monitors external factors that shape tissue structure²⁸. *NF2* recruits core Hippo signalling pathway members (*LATS1/2*) to inhibit activation of the transcriptional cofactors YAP1 and TAZ²⁹. *RASSF7* also regulates Hippo pathways, and its overexpression promotes phosphorylation and nuclear translocation of YAP1²⁴. We found *RASSF7* amplification in 39 mesotheliomas, *NF2* mutations in 24, *LATS2* mutations in 6 and *LATS1* in 2, so that non-overlapping lesions in Hippo pathways were present in 52/121 mesotheliomas (43%) and a further 9 mesothelioma had more than one lesion (total 50%) (Fig. 2). *WNT5B* transcription, which we found increased in sarcomatoid tumours, may also induce YAP/TAZ activation through non-canonical pathways³⁰.

We did not find significant differences in transcript abundances when comparing RNA-sequencing derived transcriptomes for *RASSF7* amplifications to other tumours; or for lesions in Hippo signalling genes (*NF2*, *LATS1*, *LATS2*) singly or combined; or for mesotheliomas with or without *SETD* mutations. We did not detect *RASSF7* amplification in any of 19 primary cell lines examined by WGS and SNP array (Supplementary File 1_Fig. 5), which may reflect selection in culture for mesothelioma genotypes that grow independently of a fibroblast matrix.

Log ₂ Fold Change	Av. Exp	P	P Adj	Chr	Name	Description
3.66	1.95	2.23E-05	3.09E-02	1	<i>PTCH2</i>	Patched 2 tumour suppressor, indicative of aberrant Hedgehog signalling
2.82	3.91	4.61E-05	3.64E-02	13	<i>GJB2</i>	Gap junction protein beta 2
2.78	3.53	1.15E-04	4.36E-02	12	<i>NXPH4</i>	Neurexophilin 4
2.35	1.35	1.18E-04	4.37E-02	X	<i>NHS</i>	Regulates actin remodelling and cell morphology
2.32	1.77	1.12E-04	4.32E-02	7	<i>HOXA7</i>	Transcription factor regulating morphogenesis and differentiation
1.26	3.26	1.20E-04	4.38E-02	8	<i>TRPS1</i>	Transcriptional repressor GATA binding 1
1.09	2.94	4.48E-05	3.64E-02	1	<i>C1orf112</i>	Chromosome 1 open reading frame 112
-1.06	4.79	7.90E-06	2.85E-02	10	<i>ZFYVE27</i>	Zinc finger protein
-1.11	5.89	1.18E-04	4.37E-02	16	<i>ILAR</i>	Interleukin 4 receptor
-1.11	5.30	4.78E-05	3.64E-02	10	<i>ERLIN1</i>	Binds cholesterol and regulates SREBP signalling pathway
-1.15	4.37	1.51E-05	2.85E-02	10	<i>FBXL15</i>	F-box and leucine rich repeat protein 15
-1.18	7.24	7.23E-05	3.95E-02	10	<i>WBPL1</i>	WW domain binding protein 1-like
-1.33	4.54	3.28E-05	3.43E-02	10	<i>SUFU</i>	Negative regulator of hedgehog signalling
-1.49	6.14	1.72E-05	2.85E-02	6	<i>CCND3</i>	Regulatory subunit of CDK4 or CDK6, involved in phosphorylation Rb1
-1.51	6.19	1.10E-05	2.85E-02	3	<i>DTX3L</i>	Deltex E3 ubiquitin ligase
-1.52	5.09	6.97E-05	3.95E-02	22	<i>ODF3B</i>	Differentially regulated in pathogenic CD4(+) T cells in MS
-1.55	7.58	1.05E-04	4.20E-02	10	<i>MYOF</i>	May be involved in membrane regeneration and repair
-1.58	4.43	6.91E-06	2.85E-02	18	<i>EPB41L3</i>	Erythrocyte membrane protein like
-1.63	2.83	9.32E-05	4.11E-02	17	<i>SCIMP</i>	TLR adaptor promotes cytokine production from macrophages; involved in MHC class II signalling
-2.13	4.41	9.12E-06	2.85E-02	10	<i>AVPI1</i>	Arginine vasopressin induced 1
-2.19	5.23	2.04E-05	3.09E-02	20	<i>SIGLEC1</i>	CD169: CD169 macrophages dominate antitumor immunity by presenting dead cell antigens
-2.24	5.86	7.82E-05	3.95E-02	10	<i>IFIT3</i>	IFN-independent upregulation of IFN-stimulated Genes during CMV infection
-2.27	5.68	3.33E-05	3.43E-02	12	<i>OAS2</i>	Involved in the innate immune response to viral infection
-2.67	3.10	1.09E-04	4.26E-02	17	<i>CLEC10A</i>	Specific Marker for human CD1c + dendritic cells; enhances TLR7/8-induced cytokine secretion
-2.73	1.58	1.39E-04	4.86E-02	12	<i>KLRD1</i>	CD4: Killer cell receptor, may be involved in the regulation of NK cell function
-2.97	1.89	1.76E-05	2.85E-02	1	<i>CR1</i>	Complement C3b/C4b receptor 1: found on dendritic and other cells
-3.08	2.61	4.28E-05	3.64E-02	19	<i>HSH2D</i>	Target of T-cell activation signals: TCR antigen recognition, and co-stimulation by CD28
-3.56	3.19	1.36E-04	4.82E-02	11	<i>HRASLS5</i>	HRAS like suppressor family member 5

Table 1. Genes differentially regulated with *SUFU* locus deletions.

Cell line	DNA repair		Hedgehog	Hippo	Palbociclib	Cell cycle RB1		
	Niraparib	Olaparib	Vismodegib	Verteporfin		Alisertib	Volasertib	AZD7762
	PARP inhibitors		SMO inhibitor	YAP inhibitor	CDK4/6 inhibitor	Aurora kinase inhibitor	PLK1 inhibitor	CHEK1 inhibitor
Meso-27T	7.96	10.52	31.53	1.08	> 50	3.20	6.57	0.45
Meso-33T	47.02	> 50	6.03	0.87	20.29	3.84	0.10	0.45
Meso-70T	> 50	2.88	> 50	1.2	> 50	0.15	0.04	2.02
NCI-H2052	29	27.3	13.7	10.9	> 50	0.81	0.64	2.42
A549	> 50	13.47	20.72	16.5	12.33	11.7	0.71	1.84
Met-5A	> 50	11.13	8.53	3.36	29.2	> 50	0.44	0.11

Table 2. IC₅₀ values for responses normalized to the control (DMSO), calculated by fitting a dose–response curve model in Graph Pad Prism and tabulated as concentration of drugs in μM. In cases where responses were above the highest drug concentration used in the experiment, IC₅₀ estimates are marked as > 50 μM. Values in bold depict sensitive primary cells and cell lines, where IC₅₀ to compounds < 10 μM and R² (goodness of fit of curve) > 0.7).

Investigation of somatic mutations confirms the major driver genes in mesothelioma. WES in 50 tumours (mean coverage 136X; 21 with paired peripheral blood lymphocyte DNA (PBL)) revealed no major loci beyond those previously described^{4,5} (Supplementary File 2_Table 2). We successfully completed TC-NGS in 119 patients (Supplementary File 2_Table 3 and Supplementary File 1_Fig. 1b), 77 of which had paired PBL, achieving a mean coverage of 792X for tumours and 802X for PBL. *BAP1* was mutated in 39 subjects (33%); *NF2* in 24 subjects (20%); *TP53* in 9 subjects (8%) and *SETD2* in 7 subjects (6%) (Fig. 2 and Supplementary File 1_Fig. 2). Mutations were scattered across coding regions of these genes (Supplementary File 1_Fig. 3b-d), consistent with their putative role as tumour suppressors.

We found two *NRAS* mutations at known oncogenic RAS hotspots (G12V and Q61H). Both mutations were found in sarcomatoid subtype tumours that did not have alterations in *CDKN2A*, *BAP1* or *NF2*. In the TCGA-Meso cohort, only one patient with biphasic histology had a G12C *KRAS* hotspot mutation with a concurrent *TP53* mutation but without alterations in other mesothelioma drivers, similar with our cohort. In the Bueno et al.⁵ cohort also only one patient with sarcomatoid subtype had a Q61K *NRAS* mutation but this was detected simultaneously with a *BAP1* frameshift mutation. We also identified three other RAS pathway related genes by WES: a *NF1* stop mutation (c.6439C>T, p.Q2147*), a splice site *RASA1* mutation (c.829-1_858.del) and a *HRAS* in-frame deletion (c.187_189del, p.E63del).

TP53 mutations carried a worse prognosis compared with *TP53* wild-type counterparts (mean OS 5.7 vs. 13.6 months, $P=0.0005$), as previously described⁵. We did not detect significant associations of other mutations with survival.

Combined analysis of CNA, WES and TC-NGS (Fig. 2) showed *CDKN2A* deletion to be present in 60% of tumours; *BAP1* mutated or deleted in 54%; *RASSF7* amplification in 33%; *RB1* deleted or mutated in 26%; *NF2* mutated in 20%; *TP53* mutated in 8%; *SETD2* in 6%; *DDX3X* in 5% and *LATS2* in 5%.

We detected a missense germline mutation localized in the UCH domain of *BAP1* from one patient with epithelioid subtype (Supplementary File 1_Fig. 3b). In other subjects, single deleterious germline mutations were found in *MSH5* and *MSH6* (representing the mismatch-repair (MMR) pathway), *RB1*, *SETD6* and *BRCA2*.

***BAP1* is the most common mutated gene in mesothelioma and is associated with up-regulation of *RET*.** We explored the effects of genetic alteration by comparing RNA-sequencing samples with and without specific genetic alterations. When compared to other tumours, *BAP1* mutations or deletions were associated ($P_{adjusted}<0.05$) with up-regulation of the *RET* proto-oncogene³¹ and *NNAT*. *NNAT* overexpression is associated with poor outcome in multiple cancers³² (Supplementary File 1_Table 6). We replicated the negative association of *BAP1* with *RET* to be present also in the Bueno et al.⁵ ($r=-0.32$, $P=2.2E-06$) and TCGA-Meso⁴ ($r=-0.45$, $P=1.3E-06$) datasets.

Mutational signatures 1 and 3 are prevalent in mesothelioma. A median of 31 non-synonymous somatic mutations per tumour exome were present in the 21 WES paired samples, consistent with the low rate observed by Bueno et al.⁵. We observed a similar low tumour mutational burden in the 77 paired samples that underwent targeted capture sequencing (Supplementary File 1_Fig. 3i).

One patient (NCMR035) had a hypermutated tumour (167 somatic mutations from WES) (Supplementary File 1_Fig. 6), accompanied by a frame-shift deletion in *MSH6* (p.Phe1104LeufsX11) and a frame-shift insertion in *PALB2* (p.Met1049AspfsX4). *PALB2* encodes a protein that recruits *BRCA2* and *RAD51* at the site of double-strand breaks³³ and plays a critical role in homologous recombination repair.

The mutation spectrum was characterized by C>T transitions, in both WES and TC-NGS panel data (Supplementary File 1_Fig. 3 and 3a respectively), consistent with earlier reports^{4,5}. Analysis of mutational signatures^{34,35} found COSMIC signatures 1 and 3 to be prevalent in the 21 paired WES samples (Supplementary File 1_Fig. 3e, f) and in WGS from 19 PMCC¹² (Supplementary File 1_Fig. 3g, h).

Signature 3 is indicative of DNA damage and failed breakpoint repair³⁵. In other cancers, signature 3 mutations often accompany biallelic inactivation of *BRCA1* or *BRCA2*, where the inability to repair DNA predicts good responses to platinum therapy. Mesothelioma responds poorly to such therapies, and we hypothesise that signatures of DNA damage may follow the actions of asbestos in the progenitor neoplastic cell.

***WNT5B* is higher expressed in sarcomatoid tumours.** We did not see any significant associations between common lesions and histological subtypes. RNA-sequencing however revealed differential transcription between histologies (Supplementary File 1_Table 4). As reported previously⁵, *WNT5B* had higher expression in sarcomatoid and mixed histology tumours compared to epithelioid tumours. Other genes significantly upregulated ($P_{adjusted}<0.001$) in non-epithelioid tumours included *GPR176* which acts as a circadian pacesetter³⁶, and known adverse factors for other cancers such as *IGF2BP1*, *CCBE1*, *HS3ST3A1*, *TRAM2* and *SERTAD2*.

High level of *VISTA* is frequent in epithelioid mesothelioma and its expression level correlates with Hedgehog and immune pathway components. We tested how the most frequent genomic alterations, *BAP1* mutation and *CDKN2A* deletion, were translated at protein levels. We stained a subset of 28 tumours (Fig. 3a) with antibodies against *BAP1* and *MTAP* (as a potential surrogate marker for *CDKN2A* deletion) along with PD-L1, *VISTA*, Ki-67 and an antibody for mitotic count (Fig. 3b-e).

BAP1 staining revealed general or focal loss in 17/28 (61%) of cases, which only partially associated with *BAP1* mutation or deletion ($P=0.01$) (Fig. 3f), as previously suggested³⁷. There was significant difference when comparing *MTAP* H-score between *CDKN2A/MTAP* deleted and wild-type samples ($P=0.001$) (Fig. 3g). The mitotic count and Ki-67 (both indicators of proliferation) correlated with each other ($P<0.0001$, $r=0.42$). Ki67

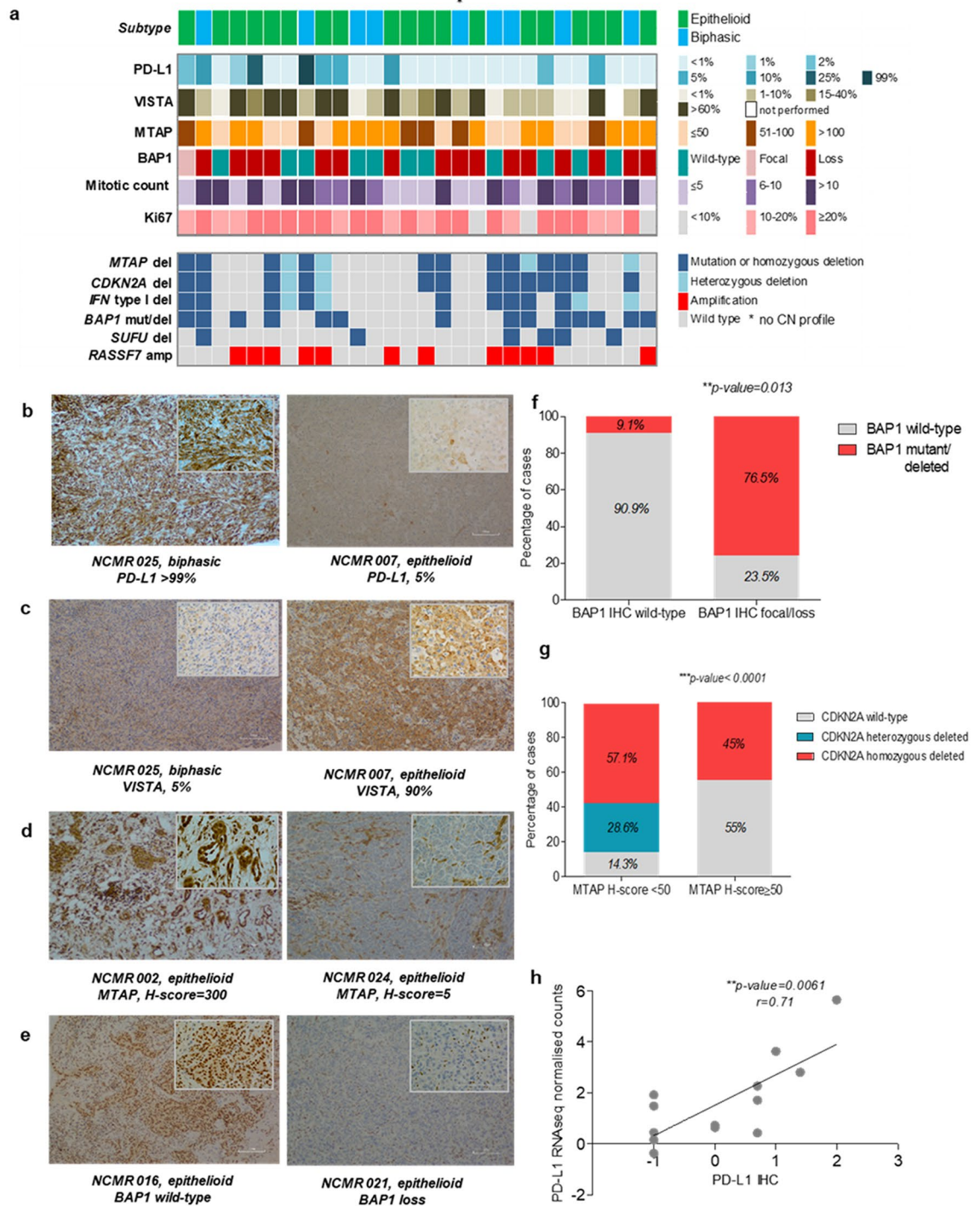


Figure 3. Histologic features of pleural mesothelioma. **(a)** Oncoplot of IHC staining and common genomic alterations; three colour coded panels are shown: the upper panel represents the histological subtype of the samples, the middle panel shows antibody staining for the proteins denoted on the left hand side of the panel (antibody staining were assessed as percentages, with the exception of BAP1; representation in the figure was done by grouping samples based on different percentage ranges that are shown in the legend on the right hand side of the panel) and the bottom panel shows any genomic alteration (mutation or copy number alteration) in the analysed samples; **(b-e)** Representative IHC images for PD-L1, MTAP and BAP1 (100×); **(f)** Analysis on BAP1 genomic and proteomic status by Fishers` exact test; **(g)** Analysis of MTAP H-score in *CDKN2A/MTAP* deleted vs *CDKN2A/MTAP* wild-type by Fisher`s exact test, with a threshold for MTAP H-score set at 50; **(h)** Spearman correlation between *PD-L1* gene expression and IHC.

correlated with copy number burden ($P=0.03$, $r=0.42$) and with MTAP score ($P=0.04$, $r=0.39$), consistent with disordered cellular division accompanying *CDKN2A* deletion.

Checkpoint inhibitors targeting PD-1 and its ligand PD-L1 cause marked tumour regression in some patients with mesothelioma³. However, PD-L1 is expressed at a low level, if at all, in most mesothelioma cases and its status imperfectly predicts response to immune checkpoint inhibitors³.

In our tumours, IHC staining for PD-L1 was also low, with only 4/28 cases (14%) exhibiting $\geq 10\%$ expression, including one case $> 70\%$. There was a good correlation between PD-L1 (SP263) staining and transcript abundance ($P<0.01$, $r=0.7$) (Fig. 3h). We did not see a consistent relationship between any Hedgehog-related transcripts and PD-L1 in transcriptomic data (Supplementary File 1_Table 5).

High-level staining of the alternative immune-checkpoint protein VISTA (V-domain Ig suppressor of T cell activation)³⁸ has been observed in epithelioid mesothelioma, and implies a better prognosis^{4,39}. We confirmed a high level of VISTA by IHC in our samples (Fig. 3a), and in RNA-sequencing data replicable associations were seen between VISTA and *SUFU*, *PTCH1*, *PTCH2*, *KLRD1* and *CR1* (Supplementary File 1_Table 5).

Drug-testing shows that primary cell models of mesothelioma are sensitive to cell cycle targeted drugs.

We explored potential therapeutic pathways that had been suggested by our genomic findings by determining the half maximal inhibitory concentration (IC_{50}) of selected compounds with three PMCC¹² that had been whole-genome sequenced (Supplementary File 1_Fig. 5). We assessed by Western blots if deletions or mutations of the main mesothelioma drivers were translated to protein levels (Supplementary File 1_Fig. 7a). For comparison, we included an immortalized mesothelioma cell line (H2052), a lung adenocarcinoma cell line (A549), and a transformed normal mesothelial cell line (Met-5A). We exposed cells to a range of drug concentrations (0.0005 to 50 micromolar (μM)) using as controls DMSO treated cells (Supplementary File 1_Fig. 7b-g).

As we had observed mutation signatures associated with repair of DNA double-strand breaks (COSMIC mutational signature 3), we tested two PARP inhibitors (Niraparib and Olaparib) that are effective in homologous repair deficiency⁴⁰. Despite reports suggesting utility in mesothelioma⁴¹, we did not see a consistent inhibition of primary cell growth (Table 2). Our results are supported by a recent report by Fennell et al.⁴² that tested Rucaparib, a third PARP inhibitor, in *BAP1* or *BRCA1* defective mesothelioma patients. Although the clinical trial achieved its endpoints, the author suggested that there is no correlation between *BAP1* or *BRCA1* expression and patients' objective response to Rucaparib.

Another tested drug in our screen, Palbociclib, PD0332991, a CDK4/CDK6 inhibitor, that is supposed to target the most frequent deletion in mesothelioma, *CDKN2A*, showed only minor effects in our cell lines (Table 2).

RB1 deletion has recently been shown to confer a robust and selective vulnerability to drugs that target DNA damage checkpoint (*CHEK1*) and chromosome segregation proteins such as Polo-Like-Kinase 1 (*PLK1*)⁴³. *CHEK1* is over-expressed in mesothelioma⁴⁴, and RNAi screens have shown mesothelioma lines to be sensitive to *CHEK1* and *PLK1* knockdown. *RB1* deficient tumours are hyper-dependent on Aurora kinase B (AURKB) for survival⁴⁵, and AURKB inhibitors are efficacious against *RB1* deficient lung cancers at non-toxic doses⁴⁵. Consistent with these observations, we found micromolar (μM) to sub- μM responses when treating with an Aurora Kinase inhibitor (Alisertib, MLN8237); an inhibitor of *PLK1/2/3* that induces G2/M arrest and apoptosis (Volasertib, BI6727)⁴⁶, and a *CHEK1/2* inhibitor that abrogates the G2/S checkpoint (AZD7762).

The involvement of Hippo pathways in our results supports previous suggestions that YAP1 axis inhibition may be used in mesothelioma therapy²⁹. We found μM IC_{50} responses to the YAP inhibitor Verteporfin in all mesothelioma cell lines (Table 2). Notably, immortalised Met-5A mesothelial cells that are not deficient in *NF2* also responded.

Discussion

In our study we have extended previous genomic analyses by testing copy number aberrations (CNAs) through SNP genotyping arrays together with WES and targeted capture sequencing. We found genetic lesions to be enriched in *RB1*/cell-cycle, Hippo and Hedgehog pathways, and identified two major immunological influences. We assessed vulnerabilities of mesothelioma tumours by testing drugs that target altered pathways or their members in whole genome sequenced primary mesothelioma cells.

The most frequent genomic alteration in our subjects was deletion of the *CDKN2A* locus on 9p21.3, found in 60% of the analysed samples. This deletion predicts a worse OS than tumours without the deletion⁴⁷. We observed that tumours with this deletion had a higher copy number burden compared with *CDKN2A* wild type patients, consistent with cell cycle dysregulation.

Hippo pathway activation was observed in more than 50% of mesothelioma tumours while Hedgehog pathway activation, as *SUFU* deletion, was seen in 21% of the tumours.

Cdkn2a deletion and Hedgehog and Hippo pathway activation have been observed in murine models of asbestos exposure well before tumour development^{7,8,19}. Our results and the remarkable consistency of genetic lesions in mesothelioma in humans^{4,5} and in mice^{7,8} suggest a hypothesis that recurrent mesothelioma break-points and mutations occur in regions of chromatin that have been accessed during the inflammatory response to asbestos. Activation of Hedgehog might also contribute to the stroma-rich microenvironment that characterises mesothelioma tumours.

Our finding of *RB1* deletions in 34% of tumours with *CDKN2A* deletion makes responses to CDK4/CDK6 antagonists less likely and underpins our finding that the CDK4/CDK6 inhibitor Palbociclib had marginal effects on primary cell survival. However, we note a previous publication has reported mesothelioma cell lines to be sensitive to this compound⁴⁸ and further investigations are indicated.

We therefore tested compounds downstream of *RB1* and showed that *RB1* defective primary cells responded well (irrespective of *CDKN2A* deletion) to an Aurora Kinase inhibitor (Alisertib, MLN8237); an inhibitor of

PLK1/2/3 that induces G2/M arrest and apoptosis (Volasertib, BI6727) and a *CHEK1/2* inhibitor (AZD7762). These findings encourage the clinical investigation of these or related compounds, and a Phase II Trial of Alisertib in salvage malignant mesothelioma is currently under way (NCT02293005).

We identified a recurrent novel amplification of *RASSF7* in 31% of tumours. Taken with other Hippo pathway members (*NF2*, *LATS1* and *LATS2*), 50% of tumours had at least one lesion of this pathway. Our testing of primary cells revealed micromolar responsiveness of mesothelioma to the YAP inhibitor Verteporfin, although it did not seem to depend on the presence of *NF2* or other Hippo mutations. These results are consistent with recent studies that have shown Verteporfin to be effective in vitro against mesothelioma cells^{49,50}.

BAP1 is the archetypal mesothelioma gene⁵¹ and was mutated in 31% of tumours and deleted in 33%. We gained some insight into its function by comparing transcriptome abundances between *BAP1* mutation/deletion and *BAP1* wild type tumours, where we found replicated up-regulation of the *RET* proto-oncogene. These results suggest tumour suppressor activities of *BAP1* beyond deubiquitination⁵². It may be of interest that *RET* inhibitors are effective in *RET*-driven NCSLC and thyroid cancers⁵³.

An important finding of our study was deletion of the *SUFU* locus on chromosome 10q24.32 in 21% of tumours. However, we did not find *SUFU* deletions in primary cells and Vismodegib, a Hedgehog inhibitor, was efficient in only one primary cell line. Beneficial effects of Vismodegib on tumour-stromal interactions have previously been shown²⁷, and a role for Hedgehog pathways in mesothelial-matrix interactions (as opposed to simple driving of cell division) is further suggested by our findings of the upregulation of *PTCH2*, *GJB2*, *NHS* and *HOXA7* in *SUFU* deleted tumours (Table 1). These results encourage the speculation that Vismodegib may be of clinical use to modify mesothelioma fibrosis. Together with *SUFU*, two other genes were deleted at the same locus, *ARL3* and *TRIM8*, the latter being involved in innate immunity.

A striking novel finding in RNA-sequencing expression data of tumours with *SUFU* locus deletion was the downregulation of T-cell and antigen-presenting cell genes (Table 1). Although unexpected, these findings were strongly replicated in other data (Supplementary File 1_Table 5) and are consistent with the known central function of Hedgehog signalling in T-cells at the immunological synapse^{54,55}.

High levels of VISTA, an alternative checkpoint inhibitor, have previously been reported in mesothelioma and confer a better outcome^{4,39}. We confirmed the strong staining for VISTA by IHC and found that VISTA abundance strongly correlated with other *SUFU*-affected immune-synapse genes. By contrast, PD-L1 staining was generally weak in the tumours. A small molecule inhibitor against VISTA (CA-170)⁵⁶ is currently in a Phase I clinical trial (NCT02812875), and our findings may provide biomarkers as well as a stimulus further to investigate VISTA therapeutic blockade in mesothelioma.

In the same context, Vismodegib might be considered as an adjuvant to immunotherapy in the presence of *SUFU* deletion. It will be relevant to test if aberrant Hedgehog immune signalling is detectable in other malignancies.

It may also be of interest that the Type I Interferon genes on 9p21.3 were deleted in 52% of all mesothelioma. Interferons induce complex pro-inflammatory responses within tumour cells as well as in accessory immune cells^{57,58}. Homozygous deletion of *IFN* genes is associated with poor response to CTLA4 blockade in patients with malignant melanoma⁵⁹. Historically, administration of IFNA2 to patients with mesothelioma has occasionally induced complete regression^{60,61}. Supplementary, early stage trials suggest that intra-pleural infection with viral vectors containing *IFNA2*⁶² or *IFNB1*⁶³ induce inflammation and encourage beneficial mesothelioma responses, suggesting an adjuvant role for interferons in therapy.

The association of *CDKN2A* deletion with higher copy number burdens might indicate a beneficial effect of immune checkpoint inhibitors, but the co-deletion of *IFN* type I could enhance tumour cell evasion of immune surveillance. On the other hand, the deletion of *IFN* genes may encourage the use of oncolytic virus as therapies¹⁷. These alternatives could be explored in immunocompetent murine models of mesothelioma.

The results of our investigations should be interpreted in the light of several limitations. We were not powered to investigate determinants of fibrosis, an important variable feature of mesothelioma. Nevertheless, we examined tumours with tumour extent down to 20% as estimated by ASCAT analysis, compared to TCGA analysis of mesothelioma that was confined to tumours with only >70% mesothelioma cells⁴, providing a reference for one extreme of the range.

The dose of asbestos exposure is a known determinant of fibrosis, but not of mesothelioma⁶⁴. Sixty percent of our cases reported working with asbestos, but we did not have accurate estimates of exposure from a detailed occupational history or from fibre counts in unaffected lungs to include exposure as a covariate in our analysis.

Calling the presence of small or uncommon amplifications and deletions in heterogenous tumour samples may be problematic. The amplification segment sizes that we observed in the Infinium SNP array (with ~3 Kb spacing between SNPs) were on average seven times smaller than deletion segments (35.1 Kb vs. 265.8 Kb), and will have been harder to detect in the uneven coverage of WES. Nevertheless, the novel CNAs are detectable in the large Bueno et al. dataset⁵, each showing significant associations with the abundance of their transcribed RNA.

We have shown that genomic findings correlate with protein levels in histological sections of FFPE. Notably, we confirmed a high level of VISTA staining^{4,39} which our transcriptomic data shows to be related to Hedgehog aberration. We were not powered to test systematically for the determinants of histological subtypes or histological features which may be important in clinical decision making. Therefore, there is an unmet need for investigations of the relationship between histology and genomic features identified in this and other studies.

We found distinctive transcriptome changes for some common lesions (*BAP1* and *SUFU* deletion), but not for lesions in the *RB1* or *NF2* pathways. This may be due to lack of power, or possibly to differences in gene expression that result from either acceleration or braking of cellular division.

We tested tool therapeutic compounds as monotherapy in patient-derived low-passage mesothelioma cells. We selected primary cells and cell lines for the drug screen to include the main histological subtypes of mesothelioma and to cover the main drivers of mesothelioma. Although the cell lines contained the most common

mutations, some CNAs, such as *RASSF7* amplification were not found. We speculate that they may have been lost by weaning of pure mesothelioma cultures from other cell types. Compounds were chosen for testing to target the pathways shown by our genomic analysis. The known interactions of mesothelioma with stroma suggest better understanding of a wider range of drug effects may come from 3D models that include fibroblasts and immune cells.

Conclusions

In conclusion, our analyses suggest roles for Aurora Kinase, PLK, CHEK and YAP inhibitors in the treatment of mesothelioma growth. *IFN* Type I and *SUFU* deletions as biomarkers may guide more effective immunotherapies. VISTA inhibition may directly modify immune recognition of mesothelioma, and an adjuvant role in immunotherapy seems possible for Hedgehog inhibitors. The involvement of Hippo and Hedgehog signals and the intense fibrosis seen clinically assert a central role for tumour-matrix interactions in the pathogenesis of mesothelioma and suggest therapeutic avenues beyond tumour cell killing.

Methods

Sample collection. Thirty unpaired tumour samples were obtained from the NIHR-BRU Advanced Lung Disease Biobank and Royal Brompton and the Harefield NHS Trust (RBH) Diagnostic Tissue Bank (NRES:10/H0504/9 and 10/H0504/29-NRES Committee Southampton and South West Hampshire) from non-consecutive surgical biopsy samples between 2006 and 2011. Eighty-two paired (tumour and blood) and 4 unpaired tumour samples were obtained from Mesobank UK, Cambridge (NRES:13/EE/0169- East of England—Cambridge Central Research Ethics Committee). Seven additional paired samples were obtained from the EQUALITY study (NRES:10/H0808/53- NRES Committee London-Dulwich). Samples were not collected sequentially or at set times, and the Mesobank specimens came from multiple centres. Tissues were collected during open or thorascopic surgical procedures prior to any anti-cancer treatment and were immediately snap frozen with or without RNAlater. Formalin-fixed paraffin embedded tissues were sectioned, stained with routine haematoxylin and eosin, and reviewed by two experienced pathologists to verify tumour histology and abundance. For RBH and EQUALITY tumours, tissues with 30% or more viable-appearing malignant cells were selected for whole exome sequencing (WES). Mesobank samples were selected to contain only tumours with > 50% malignant cells on histology. Supplementary File 2_Table 1 contains a summary of patients' clinico-pathologic details. All experiments were performed in accordance with ethical guidelines and all participants gave an informed written consent.

Genomic DNA isolation and quality control. Genomic DNA was isolated from frozen tumour tissues and matched normal tissue (blood) with routine methods (Qiagen DNA and RNA extraction kits, Qiagen, Hilden, Germany). DNA yield and purity were assessed with the Quant-iT™ PicoGreen dsDNA Assay Kit (Life Technologies, Carlsbad, USA) or Qubit 3.0 fluorimeter (Thermo Scientific, Massachusetts, USA) according to manufacturers' protocols.

Whole exome sequencing (WES). WES was performed at the McGill Genome Centre, Canada. Genomic DNA from tumour and blood samples were fragmented and hybridised as per SureSelect^{XT} Target Enrichment System (Agilent SureSelect Human All Exon V4) for the Paired-End Multiplex Sequencing protocol. The captured libraries were sequenced on an Illumina HiSeq2000 according to standard protocols. Supplementary File 2_Table 2 contains a list of somatic variants identified from whole exome sequencing.

Targeted capture sequencing of a custom gene panel. The entire coding regions of fifty-seven genes were included in a hybridisation capture panel (Supplementary File 1_Table 1), based on: recurrence in our WES tumour set; reported in the Catalogue of Somatic Mutations in Cancer (COSMIC) database; implicated in cancer⁶⁵, or reported in the TCGA or Bueno et al. studies^{4,5}. Sequencing libraries were prepared from DNA extracted from tumours and normal tissue (whole blood) samples using the SureSelect QXT Target Enrichment System (Agilent, Santa Clara, USA) according to the manufacturer's protocols. Sequencing was performed on a MiSeq or NextSeq500/550 platform (Illumina) with a mean read depth of 780.6X (all samples). Supplementary File 2_Table 3 contains a list of filtered somatic variants from targeted capture sequencing.

Data processing and quality control. Raw fastq files were quality checked before alignment with BWA mem (v 0.7.12). GATK software (v 3.8 and 4.1) was used to refine the alignment data before variant calling. For Targeted capture sequencing (TC-NGS), somatic and germline variant calling was performed for the paired samples using VarScan software (v 2.4.2). For the un-paired samples, joint variant calling was performed using Platypus (v 0.8.1). In case of WES, joint variant calling was performed at McGill using the GATK Haplotype-Caller.

Detection of candidate pathogenic somatic and germline variants. Candidate somatic and germline variants were checked for presence in population data (gnomAD (genome Aggregation Database) genomes and exomes (rel.2.0.1) and the ExAC (Exome Aggregation Consortium) non-TCGA rel.0.3.1 resources) and those with frequency $\geq 10^{-3}$ were deemed to be polymorphisms and filtered out. Additional selection was based on either being assigned as High or Moderate impact by VEP⁶⁶ or predicted to be splice-site altering (dbSNV⁶⁷ score of >0.6). Further prioritisation of SNV (single nucleotide variant) candidates was done based on predicted deleteriousness by at least two of three algorithms from SIFT, Polyphen and MutationTaster.

Copy-number analysis. One hundred and twenty-one DNA samples were interrogated at Eurofins against the Human Infinium Omni-Express-Exome v 1.3 and v 1.4 Bead Chips (Illumina) arrays containing >950 K markers, using microarray technology. One hundred and eighteen samples remained (77 paired and 43 unpaired) after QC checks. Raw copy number data (LRR and BAF) were exported from GenomeStudio software (v 1.9.4). GC correction was performed to account for genomic wave artefacts affecting SNP arrays using ASCAT (v 2.4.4). The GC corrected Log R ratios (LRR) were then processed using DNACopy (v 1.52) for segmentation and filtered for marker support. Recurrent germline CN segments were identified and subtracted from the tumour sample CN segments. Germline subtracted copy number segments were then processed with GISTIC (v 2.0.23). Plotting of GISTIC results was done in maftools (v 1.4.28). Copy number burden was defined as the percentage of the genome carrying copy number aberration. Additional information can be found in Supplementary File 1_Supplementary Materials and methods.

Mutation signature analysis. Somatic single nucleotide variants (SNVs) from the 21 paired WES samples were analysed for tri-nucleotide frequency around the mutated base using MutationalPatterns⁶⁸ in R. The Sanger COSMIC signature panel (n = 30) was used to infer mutational processes by obtaining the percentage contribution of 30 signatures per sample. Only signatures contributing to >25% of samples were carried forward. Paired germline samples were not available for whole-genome sequencing (WGS) of 19 mesothelioma primary cells (PMCC) (one mesothelioma primary cell WGS had failed QC), and so annotation-assisted filtering of the total SNVs was done. Only those SNVs that were non-polymorphic and either protein-sequence altering or predicted to be splice-site altering, were considered and analysed as described for the tumour tissue samples (Supplementary File 1_Fig. 6).

RNA sequencing. Total RNA was isolated from 35 tumours using the RNEasy Fibrous Midi kit (Qiagen, Hilden, Germany) following the manufacturer's protocol. Concentration and quality were determined with the 2100 Bioanalyzer and Total RNA Nano kit (Agilent Technologies, California, United States) as per manufacturer's instructions. RNA sequencing was performed at McGill Genome Centre.

Replication in published data. A supplementary panel of 99 paired mesothelioma samples analysed by whole-exome sequencing (WES) and published by Bueno et al.⁵ was downloaded to investigate the presence of CNAs for *RASSF7*, *RB1* and *SUFU*. The concurrent RNA-sequencing (RNA-seq) (98 of the WES samples) was also investigated for expression change in the direction of copy-number. Raw fastq reads were accessed from the EGA repository (EGAS00001001563). After quality-checking sequences were aligned using BWA MEM⁶⁹ and STAR⁷⁰ for WES and RNA-seq data respectively. CNVkit⁷¹ was used to estimate CN calls. Mann–Whitney tests were used for comparisons between CNA versus CNA neutral samples.

Immunohistochemistry. Three µm whole slide FFPE tumours sections mirroring fresh frozen tissue used for molecular analysis underwent H&E staining according to routine histopathological protocols. Further sections underwent staining for BAP-1 (Santa Cruz BioTechnology, clone C4), Ki67 (Ventana, 30-9), MTAP (NovusBio, 2G4), PD-L1 (Ventana, SP263) and VISTA (D1L2G, Cell Signalling Technology). Mitotic activity was evaluated by counting the number of mitotic figures in the area of highest activity, over 10 high powered fields (0.24 mm²).

Whole genome sequencing of primary cell lines. Genomic DNA extracted from patient derived mesothelioma cell lines (n = 20, of which one failed QC) and primary normal mesothelial cells, MES-F (purchased from ZenBio, USA) underwent WGS (McGill) and SNP genotyping (Eurofins). Genomic details of the commercial cell line were obtained from published data (COSMIC, CCLE databases, 61). Supplementary File 2_Table 4 contains a list of variants from whole genome sequencing for the primary cells.

In vitro drug testing. Patient-derived primary cells, Meso-27T, Meso-33T and Meso-70T were obtained from the MRC Toxicology Unit, University of Cambridge, UK. Commercial cell lines NCI-H2052 (sarcomatoid mesothelioma), A549 (lung adenocarcinoma) and Met-5A (normal mesothelial, SV40 transformed) previously obtained from ATCC were gifted from the MRC Toxicology Unit. Original establishment of the primary cells was as previously described¹². Additional information can be found in Supplementary File 1_Supplementary Materials and Methods. All primary cells and cell lines were maintained in RPMI-1640 growth media supplemented with L-glutamine (2 mM), penicillin (100 U/ml), streptomycin (100 µg/ml) and 10% FBS at 37 °C in 5% CO₂.

Eight drugs were investigated, based on our results. These were Niraparib (MK-4827, HY-10619, MedChem Express), Olaparib (HY-10162, MedChem Express), Palbociclib, PD0332991 (A8316, ApexBio), Alisertib (MLN8237, S1133, Selleckchem), Volasertib (BI6727, S2235, Selleckchem), Vismodegib (GDC-0499, S1082, Selleckchem), AZD7762 (S1532, Selleckchem) and Verteporfin (SML0534, Sigma Aldrich). All drugs were diluted in DMSO and aliquots maintained at -20 °C. Drug aliquots were freeze-thawed no more than three times. For all experiments, controls consisted of DMSO-alone treated primary cells or cell lines.

Cells were seeded in 96-well plates (4 × 10³ cells/well) 24 h prior to drug treatments. Each line was treated for six days (except for drug PD0332991 where treatment was 3 days) with a range of concentrations from 0.0005 to 50 µM. Cell viability was measured with MTS assay (CellTiter 96[®] AQueous One Solution Cell Proliferation Assay, Promega) on a plate reader (Tecan).

Three independent experiments, each having three technical replicates, were conducted for each drug tested. Results are represented as the average normalized to the control at each time point (mean \pm S.E.M.). Briefly, the raw optical densities obtained from each well were normalized to the average of DMSO control wells, that was considered 100% viability (maximal DMSO concentration used was 0.5%). IC₅₀ values were calculated with Graph Pad Prism 5 software (GraphPad Software Inc, San Diego, CA) using a dose–response curve fit model using the nonlinear log (inhibitor) versus response-variable slope (four parameters) equation. In addition, the IC₅₀ values were only considered if the software gave unambiguous results and the R² value was > 0.7.

Statistical analysis. Categorical variables were evaluated using Fisher's exact test for two-by-two comparison or Pearson's χ^2 for comparison that exceeded the two-by-two condition. Differences between groups were evaluated by means of nonparametric Mann–Whitney or Kruskal–Wallis test.

Clinical outcomes. Overall survival (OS), defined as time from date of diagnosis to time of death, was available for 110 patients. OS was estimated using the Cox–Mantel log-rank test, Kaplan–Meier method. Censoring of OS was done at the date of the last follow-up if death did not occur. Survival analyses were performed using the long-rank Kaplan–Meier and the differences in survival curves were assessed by Mantel Cox Log rank test. A $P \leq 0.05$ was considered statistically significant and noted as: * $P \leq 0.05$, ** $P \leq 0.01$, *** $P \leq 0.001$. Tests and graphs were performed with Graph-Pad Prism 5, SPSS Statistics 25 or R Studio.

Ethics approval and consent to participate. All samples were collected and used under ethic and consented approval to participate in the study. Thirty unpaired tumour samples were obtained from the NIHR-BRU Advanced Lung Disease Biobank and Royal Brompton and the Harefield NHS Trust (RBH) Diagnostic Tissue Bank (NRES:10/H0504/9 and 10/H0504/29-NRES Committee Southampton and South West Hampshire) with eighty-two paired (tumour and blood) and 4 unpaired tumour samples obtained from Mesobank UK, Cambridge (NRES:13/EE/0169-East of England—Cambridge Central Research Ethics Committee). Seven Supplementary paired samples were obtained from the EQUALITY study (NRES:10/H0808/53-NRES Committee London-Dulwich).

Data availability

The datasets generated and/or analysed during the current study have been submitted at the European Genome-Phenome Archive (EGA) (<https://ega-archive.org/>) under accession code: EGAS00001004845.

Received: 23 March 2021; Accepted: 2 September 2021

Published online: 27 September 2021

References

1. Odgerel, C. O. *et al.* Estimation of the global burden of mesothelioma deaths from incomplete national mortality data. *Occup. Environ. Med.* **74**, 851–858. <https://doi.org/10.1136/oemed-2017-104298> (2017).
2. Disselhorst, M. J. *et al.* Ipilimumab and nivolumab in the treatment of recurrent malignant pleural mesothelioma (INITIATE): Results of a prospective, single-arm, phase 2 trial. *Lancet Respir. Med.* **7**, 260–270. [https://doi.org/10.1016/S2213-2600\(18\)30420-X](https://doi.org/10.1016/S2213-2600(18)30420-X) (2019).
3. Scherpereel, A. *et al.* Nivolumab or nivolumab plus ipilimumab in patients with relapsed malignant pleural mesothelioma (IFCT-1501 MAPS2): A multicentre, open-label, randomised, non-comparative, phase 2 trial. *Lancet Oncol.* **20**, 239–253. [https://doi.org/10.1016/S1470-2045\(18\)30765-4](https://doi.org/10.1016/S1470-2045(18)30765-4) (2019).
4. Hmeljak, J. *et al.* Integrative molecular characterization of malignant pleural mesothelioma. *Cancer Discov.* **8**, 1548–1565. <https://doi.org/10.1158/2159-8290.CD-18-0804> (2018).
5. Bueno, R. *et al.* Comprehensive genomic analysis of malignant pleural mesothelioma identifies recurrent mutations, gene fusions and splicing alterations. *Nat. Genet.* **48**, 407–416. <https://doi.org/10.1038/ng.3520> (2016).
6. Rintoul, R. C., Rassl, D. M., Gittins, J. & Marciniak, S. J. Mesobank UK: An international mesothelioma bioresource. *Thorax* **71**, 380–382. <https://doi.org/10.1136/thoraxjnl-2015-207496> (2016).
7. Chernova, T. *et al.* Long-fiber carbon nanotubes replicate asbestos-induced mesothelioma with disruption of the tumor suppressor gene Cdkn2a (Ink4a/Arf). *Curr. Biol.* **27**, 3302–3314 e3306. <https://doi.org/10.1016/j.cub.2017.09.007> (2017).
8. Rehrauer, H. *et al.* How asbestos drives the tissue towards tumors: YAP activation, macrophage and mesothelial precursor recruitment, RNA editing, and somatic mutations. *Oncogene* **37**, 2645–2659. <https://doi.org/10.1038/s41388-018-0153-z> (2018).
9. Liu, W., Ernst, J. D. & Broadus, V. C. Phagocytosis of crocidolite asbestos induces oxidative stress, DNA damage, and apoptosis in mesothelial cells. *Am. J. Respir. Cell Mol. Biol.* **23**, 371–378. <https://doi.org/10.1165/ajrcmb.23.3.4094> (2000).
10. Upadhyay, D. & Kamp, D. W. Asbestos-induced pulmonary toxicity: Role of DNA damage and apoptosis. *Exp. Biol. Med.* (Maywood) **228**, 650–659 (2003).
11. Huret, J. L. *et al.* Atlas of genetics and cytogenetics in oncology and haematology in 2013. *Nucleic Acids Res.* **41**, D920–924. <https://doi.org/10.1093/nar/gks1082> (2013).
12. Chernova, T. *et al.* Molecular profiling reveals primary mesothelioma cell lines recapitulate human disease. *Cell. Death Differ.* **23**, 1152–1164. <https://doi.org/10.1038/cdd.2015.165> (2016).
13. van der Bij, S. *et al.* Prognosis and prognostic factors of patients with mesothelioma: A population-based study. *Br. J. Cancer* **107**, 161–164. <https://doi.org/10.1038/bjc.2012.245> (2012).
14. Mermel, C. H. *et al.* GISTIC2.0 facilitates sensitive and confident localization of the targets of focal somatic copy-number alteration in human cancers. *Genome Biol.* **12**, R41. <https://doi.org/10.1186/gb-2011-12-4-r41> (2011).
15. Lopez-Rios, F. *et al.* Global gene expression profiling of pleural mesotheliomas: Overexpression of aurora kinases and P16/CDKN2A deletion as prognostic factors and critical evaluation of microarray-based prognostic prediction. *Cancer Res* **66**, 2970–2979. <https://doi.org/10.1158/0008-5472.CAN-05-3907> (2006).
16. Nastase, A. *et al.* MA23.10 low number of mutations and frequent co-deletions of CDKN2A and IFN type I characterize malignant pleural mesothelioma. *J. Thorac. Oncol.* **14**, S345. <https://doi.org/10.1016/j.jtho.2019.08.698> (2019).
17. Delaunay, T. *et al.* Frequent homozygous deletions of type I interferon genes in pleural mesothelioma confer sensitivity to oncolytic measles virus. *J. Thorac. Oncol.* **15**, 827–842. <https://doi.org/10.1016/j.jtho.2019.12.128> (2020).

18. Yap, T. A., Aerts, J. G., Popat, S. & Fennell, D. A. Novel insights into mesothelioma biology and implications for therapy. *Nat. Rev. Cancer* **17**, 475–488. <https://doi.org/10.1038/nrc.2017.42> (2017).
19. Felley-Bosco, E., Opitz, I. & Meerang, M. Hedgehog signaling in malignant pleural mesothelioma. *Genes (Basel)* **6**, 500–511. <https://doi.org/10.3390/genes6030500> (2015).
20. Lee, Y. *et al.* Loss of suppressor-of-fused function promotes tumorigenesis. *Oncogene* **26**, 6442–6447. <https://doi.org/10.1038/sj.onc.1210467> (2007).
21. Bhaduri, U. & Merla, G. Rise of TRIM8: A molecule of duality. *Mol. Ther. Nucleic Acids* **22**, 434–444. <https://doi.org/10.1016/j.omtn.2020.08.034> (2020).
22. Caratozzolo, M. F., Marzano, F., Mastropasqua, F., Sbisà, E. & Tullo, A. TRIM8: Making the right decision between the oncogene and tumour suppressor Role. *Genes (Basel)* <https://doi.org/10.3390/genes8120354> (2017).
23. Volodko, N., Gordon, M., Salla, M., Ghazaleh, H. A. & Baksh, S. RASSF tumor suppressor gene family: Biological functions and regulation. *FEBS Lett.* **588**, 2671–2684. <https://doi.org/10.1016/j.febslet.2014.02.041> (2014).
24. Zheng, X. *et al.* The coiled-coil domain of oncogene RASSF 7 inhibits hippo signaling and promotes non-small cell lung cancer. *Oncotarget* **8**, 78734–78748. <https://doi.org/10.18632/oncotarget.20223> (2017).
25. Okazaki, N., Takahashi, N., Kojima, S., Masuho, Y. & Koga, H. Protocadherin LKC, a new candidate for a tumor suppressor of colon and liver cancers, its association with contact inhibition of cell proliferation. *Carcinogenesis* **23**, 1139–1148. <https://doi.org/10.1093/carcin/23.7.1139> (2002).
26. Islam, M. A., Sooro, M. A. & Zhang, P. Autophagic regulation of p62 is critical for cancer therapy Int. *J. Mol. Sci.* <https://doi.org/10.3390/ijms19051405> (2018).
27. Meerang, M. *et al.* Antagonizing the hedgehog pathway with vismodegib impairs malignant pleural mesothelioma growth in vivo by affecting stroma. *Mol. Cancer Ther.* **15**, 1095–1105. <https://doi.org/10.1158/1535-7163.MCT-15-0583> (2016).
28. Nakatani, K. *et al.* Targeting the Hippo signalling pathway for cancer treatment. *J. Biochem.* **161**, 237–244. <https://doi.org/10.1093/jb/mvw074> (2017).
29. Woodard, G. A., Yang, Y. L., You, L. & Jablons, D. M. Drug development against the hippo pathway in mesothelioma. *Transl. Lung Cancer Res.* **6**, 335–342. <https://doi.org/10.21037/tlcr.2017.06.02> (2017).
30. Azzolin, L. *et al.* YAP/TAZ incorporation in the beta-catenin destruction complex orchestrates the Wnt response. *Cell* **158**, 157–170. <https://doi.org/10.1016/j.cell.2014.06.013> (2014).
31. Kato, S. *et al.* RET aberrations in diverse cancers: Next-generation sequencing of 4,871 patients. *Clin. Cancer Res.* **23**, 1988–1997. <https://doi.org/10.1158/1078-0432.CCR-16-1679> (2017).
32. Nass, N. *et al.* High neuronatin (NNAT) expression is associated with poor outcome in breast cancer. *Virchows Arch* **471**, 23–30. <https://doi.org/10.1007/s00428-017-2154-7> (2017).
33. Sy, S. M., Huen, M. S. & Chen, J. PALB2 is an integral component of the BRCA complex required for homologous recombination repair. *Proc. Natl. Acad. Sci. U. S. A.* **106**, 7155–7160. <https://doi.org/10.1073/pnas.0811159106> (2009).
34. Blokzijl, F., Janssen, R., van Boxtel, R. & Cuppen, E. MutationalPatterns: Comprehensive genome-wide analysis of mutational processes. *Genome Medicine* **10**, 33. <https://doi.org/10.1186/s13073-018-0539-0> (2018).
35. Alexandrov, L. B. *et al.* Signatures of mutational processes in human cancer. *Nature* **500**, 415–421. <https://doi.org/10.1038/nature12477> (2013).
36. Doi, M. *et al.* Gpr176 is a Gz-linked orphan G-protein-coupled receptor that sets the pace of circadian behaviour. *Nat. Commun.* **7**, 10583. <https://doi.org/10.1038/ncomms10583> (2016).
37. Righi, L. *et al.* BRCA1-associated protein 1 (BAP1) Immunohistochemical expression as a diagnostic tool in malignant pleural mesothelioma classification: A large retrospective study. *J. Thorac. Oncol.* **11**, 2006–2017. <https://doi.org/10.1016/j.jtho.2016.06.020> (2016).
38. Lines, J. L. *et al.* VISTA is an immune checkpoint molecule for human T cells. *Cancer Res.* **74**, 1924–1932. <https://doi.org/10.1158/0008-5472.CAN-13-1504> (2014).
39. Muller, S. *et al.* V-domain Ig-containing suppressor of T-cell activation (VISTA), a potentially targetable immune checkpoint molecule, is highly expressed in epithelioid malignant pleural mesothelioma. *Mod. Pathol.* **33**, 303–311. <https://doi.org/10.1038/s41379-019-0364-z> (2020).
40. Mateo, J. *et al.* A decade of clinical development of PARP inhibitors in perspective. *Ann. Oncol.* **30**, 1437–1447. <https://doi.org/10.1093/annonc/mdz192> (2019).
41. Srinivasan, G. *et al.* Synthetic lethality in malignant pleural mesothelioma with PARP1 inhibition. *Cancer Chemother. Pharmacol.* **80**, 861–867. <https://doi.org/10.1007/s00280-017-3401-y> (2017).
42. Fennell, D. A. *et al.* Rucaparib in patients with BAP1-deficient or BRCA1-deficient mesothelioma (MiST1): An open-label, single-arm, phase 2a clinical trial. *Lancet Respir. Med.* [https://doi.org/10.1016/S2213-2600\(20\)30390-8](https://doi.org/10.1016/S2213-2600(20)30390-8) (2021).
43. Witkiewicz, A. K. *et al.* Targeting the vulnerability of RB tumor suppressor loss in triple-negative breast cancer. *Cell. Rep.* **22**, 1185–1199. <https://doi.org/10.1016/j.celrep.2018.01.022> (2018).
44. Romagnoli, S. *et al.* Identification of potential therapeutic targets in malignant mesothelioma using cell-cycle gene expression analysis. *Am. J. Pathol.* **174**, 762–770. <https://doi.org/10.2353/ajpath.2009.080721> (2009).
45. Oser, M. G. *et al.* Cells lacking the RB1 tumor suppressor gene are hyperdependent on aurora B kinase for survival. *Cancer Discov.* **9**, 230–247. <https://doi.org/10.1158/2159-8290.CD-18-0389> (2019).
46. Van den Bossche, J. *et al.* In vitro study of the Polo-like kinase 1 inhibitor volasertib in non-small-cell lung cancer reveals a role for the tumor suppressor p53. *Mol. Oncol.* **13**, 1196–1213. <https://doi.org/10.1002/1878-0261.12477> (2019).
47. Illei, P. B., Rusch, V. W., Zakowski, M. F. & Ladanyi, M. Homozygous deletion of CDKN2A and co-deletion of the methylthioadenosine phosphorylase gene in the majority of pleural mesotheliomas. *Clin. Cancer Res.* **9**, 2108–2113 (2003).
48. Bonelli, M. A. *et al.* Combined inhibition of CDK4/6 and PI3K/AKT/mTOR pathways induces a synergistic anti-tumor effect in malignant pleural mesothelioma cells. *Neoplasia* **19**, 637–648. <https://doi.org/10.1016/j.neo.2017.05.003> (2017).
49. Kandasamy, S. *et al.* The YAP1 signaling inhibitors, verteporfin and CA3, suppress the mesothelioma cancer stem cell phenotype. *Mol. Cancer Res.* **18**, 343–351. <https://doi.org/10.1158/1541-7786.Mcr-19-0914> (2020).
50. Tranchant, R. *et al.* Assessment of signaling pathway inhibitors and identification of predictive biomarkers in malignant pleural mesothelioma. *Lung Cancer* **126**, 15–24. <https://doi.org/10.1016/j.lungcan.2018.10.015> (2018).
51. Testa, J. R. *et al.* Germline BAP1 mutations predispose to malignant mesothelioma. *Nat. Genet.* **43**, 1022–1025. <https://doi.org/10.1038/ng.912> (2011).
52. Ventii, K. H. *et al.* BRCA1-associated protein-1 is a tumor suppressor that requires deubiquitinating activity and nuclear localization. *Cancer Res.* **68**, 6953–6962. <https://doi.org/10.1158/0008-5472.CAN-08-0365> (2008).
53. BLU-667 controls RET-altered thyroid cancers. *Cancer Discov.* **9**, OF5. <https://doi.org/10.1158/2159-8290.CD-NB2019-084> (2019).
54. Rowbotham, N. J. *et al.* Activation of the Hedgehog signaling pathway in T-lineage cells inhibits TCR repertoire selection in the thymus and peripheral T-cell activation. *Blood* **109**, 3757–3766. <https://doi.org/10.1182/blood-2006-07-037655> (2007).
55. de la Roche, M. *et al.* Hedgehog signaling controls T cell killing at the immunological synapse. *Science* **342**, 1247–1250. <https://doi.org/10.1126/science.1244689> (2013).
56. Musielak, B. *et al.* CA-170—A potent small-molecule PD-L1 inhibitor or not?. *Molecules* <https://doi.org/10.3390/molecules24152804> (2019).

57. Borden, E. C. Interferons alpha and beta in cancer: Therapeutic opportunities from new insights. *Nat. Rev. Drug Discov.* **18**, 219–234. <https://doi.org/10.1038/s41573-018-0011-2> (2019).
58. Liu, H. *et al.* Tumor-derived IFN triggers chronic pathway agonism and sensitivity to ADAR loss. *Nat. Med.* **25**, 95–102. <https://doi.org/10.1038/s41591-018-0302-5> (2019).
59. Ye, Z. *et al.* Prevalent homozygous deletions of type I interferon and defensin genes in human cancers associate with immunotherapy resistance. *Clin. Cancer Res.* **24**, 3299–3308. <https://doi.org/10.1158/1078-0432.CCR-17-3008> (2018).
60. Christmas, T. I., Manning, L. S., Garlepp, M. J., Musk, A. W. & Robinson, B. W. Effect of interferon-alpha 2a on malignant mesothelioma. *J. Interferon Res.* **13**, 9–12 (1993).
61. Sexl, V., Wagner, L., Wiesholzer, M., Presterl, E. & Base, W. Treatment of a patient with malignant mesothelioma with interferon-alpha 2 based on in vitro sensitivity tests. *Clin. Investig.* **72**, 317–320 (1994).
62. Sterman, D. H. *et al.* Pilot and feasibility trial evaluating immuno-gene therapy of malignant mesothelioma using intrapleural delivery of adenovirus-IFNalpha combined with chemotherapy. *Clin. Cancer Res.* **22**, 3791–3800. <https://doi.org/10.1158/1078-0432.CCR-15-2133> (2016).
63. Sterman, D. H. *et al.* A phase I trial of repeated intrapleural adenoviral-mediated interferon-beta gene transfer for mesothelioma and metastatic pleural effusions. *Mol. Ther.* **18**, 852–860. <https://doi.org/10.1038/mt.2009.309> (2010).
64. Cookson, W. O. *et al.* Benign and malignant pleural effusions in former Wittenoom crocidolite millers and miners. *Aust. N. Z. J. Med.* **15**, 731–737 (1985).
65. Leiserson, M. D. *et al.* Pan-cancer network analysis identifies combinations of rare somatic mutations across pathways and protein complexes. *Nat. Genet.* **47**, 106–114. <https://doi.org/10.1038/ng.3168> (2015).
66. McLaren, W. *et al.* The ensembl variant effect predictor. *Genome Biol.* **17**, 122. <https://doi.org/10.1186/s13059-016-0974-4> (2016).
67. Jian, X., Boerwinkle, E. & Liu, X. In silico prediction of splice-altering single nucleotide variants in the human genome. *Nucleic Acids Res.* **42**, 13534–13544. <https://doi.org/10.1093/nar/gku1206> (2014).
68. Blokzijl, F., Janssen, R., van Boxtel, R. & Cuppen, E. Mutational patterns: Comprehensive genome-wide analysis of mutational processes. *Genome Med.* **10**, 33. <https://doi.org/10.1186/s13073-018-0539-0> (2018).
69. Li, H. & Durbin, R. Fast and accurate short read alignment with Burrows–Wheeler transform. *Bioinformatics* **25**, 1754–1760. <https://doi.org/10.1093/bioinformatics/btp324> (2009).
70. Dobin, A. *et al.* STAR: Ultrafast universal RNA-seq aligner. *Bioinformatics* **29**, 15–21. <https://doi.org/10.1093/bioinformatics/bts635> (2013).
71. Talevich, E., Shain, A. H., Botton, T. & Bastian, B. C. CNVkit: Genome-wide copy number detection and visualization from targeted DNA sequencing. *PLoS Comput. Biol.* **12**, e1004873. <https://doi.org/10.1371/journal.pcbi.1004873> (2016).

Acknowledgements

This study was financially supported by a Libor Fund grant from the UK Department of Health, by the British Lung Foundation and by the Asmarley Foundation. MMF, AEW, XMS and TC are funded by the UK Medical Research Council. SP acknowledges NHS funding to the Royal Marsden Hospital-Institute of Cancer Research Biomedical Research Centre. We thank Cambridge Biomedical Research Centre and Cambridge Cancer Centre.

Author contributions

W.O.C.M.C., M.F.M., M.L., S.P. and A.M.B. planned the study; A.N. processed samples and prepared libraries for targeted capture sequencing, post-analysed whole exome, T.C.-N.G.S., R.N.A. sequencing and I.H.C. data, and performed drug testing on primary cells and cell lines; A.M. performed bioinformatics analysis of whole exome and whole genome sequencing, targeted capture, RNA sequencing and copy number data; S.G. and S.K.L. processed and prepared samples for whole exome, RNA sequencing and copy number analysis; H.A. analysed WES data; D.M.R. and M.E. provided support in generating the TC-NGS panel and analysis of the libraries; A.B. performed immunohistochemistry staining, Y.Z.Z. and A.G.N. interpreted immunohistochemistry data; T.C., X-M.S., A.E.W. and M.M. established and characterized primary cells from tumours; M.L. oversaw whole-exome and RNA sequencing of the samples and advised on analyses; E.L., R.C.R. and T.B. gathered samples and associated metadata for the study; and S.P. and A.N.T. provided clinical and epidemiological scientific guidance. A.N. and A.M. wrote the first draft of the manuscript with guidance by W.O.C.M.C., M.F.M. and A.M.B., before editing by all the other authors.

Competing interests

SP reports honoraria from BMS, Roche, Takeda, AstraZeneca, Chugai, Novartis, Pfizer, MSD, EMD Serono, Guardant Health, AbbVie, Boehringer Ingelheim, and Tesaro. All other authors have no competing interests to declare.

Additional information

Supplementary Information The online version contains supplementary material available at <https://doi.org/10.1038/s41598-021-98414-w>.

Correspondence and requests for materials should be addressed to M.F.M. or W.O.C.M.C.

Reprints and permissions information is available at www.nature.com/reprints.

Publisher's note Springer Nature remains neutral with regard to jurisdictional claims in published maps and institutional affiliations.



Open Access This article is licensed under a Creative Commons Attribution 4.0 International License, which permits use, sharing, adaptation, distribution and reproduction in any medium or format, as long as you give appropriate credit to the original author(s) and the source, provide a link to the Creative Commons licence, and indicate if changes were made. The images or other third party material in this article are included in the article's Creative Commons licence, unless indicated otherwise in a credit line to the material. If material is not included in the article's Creative Commons licence and your intended use is not permitted by statutory regulation or exceeds the permitted use, you will need to obtain permission directly from the copyright holder. To view a copy of this licence, visit <http://creativecommons.org/licenses/by/4.0/>.

© The Author(s) 2021